

# ON ARRAY GEOMETRY AND SELF-INTERFERENCE IN FULL-DUPLEX MASSIVE MIMO COMMUNICATIONS

Robin Rajamäki\*<sup>†</sup> and Risto Wichman<sup>†</sup>

\*University of California, San Diego, USA; <sup>†</sup>Aalto University, Finland

## ABSTRACT

This paper studies the role of the joint transmit-receive antenna array geometry in shaping the self-interference (SI) channel in full-duplex communications. We consider a simple spherical wave SI model and two prototypical linear array geometries with uniformly spaced transmit and receive antennas. We show that the resulting SI channel matrix has a regular (Toeplitz) structure in both of these cases. However, the number of significant singular values of these matrices—an indication of the severity of SI—can be markedly different. We demonstrate that both reduced SI and high angular resolution can be obtained by employing suitable sparse array configurations that fully leverage the available joint transmit-receive array aperture without suffering from angular ambiguities. Numerical electromagnetic simulations also suggest that the worst-case SI of such sparse arrays need not increase—but can actually decrease—with the number of antennas. Our findings provide preliminary insight into the extent to which the array geometry alone can mitigate SI in full-duplex massive MIMO communications systems employing a large number of antennas.

## 1. INTRODUCTION

Full-duplex technology holds the promise of doubling the spectral efficiency of future wireless systems by utilizing the same temporal, spectral, and spatial resources for simultaneous uplink (UL) and downlink (DL) communications [1]. Indeed, FD has recently experienced a surge of renewed research interest due to the ever increasing performance demands of emerging millimeter-wave massive multiple-input multiple-output (MIMO) communications [2], and integrated sensing and communications (ISAC) systems [3].

A key technical challenge of full-duplex communications is the potentially severe *self-interference* (SI) caused by simultaneous transmission and reception at the base station (BS). Cancellation of this SI at the BS receiver may further be complicated by transmitter noise and array calibration errors. Moreover, canceling the SI digitally may be infeasible, due to the large dynamic range that would be required of the analog-to-digital converters (ADCs) at the receiver to digitize both the weak received UL signal of interest and the

strong transmitted DL signal causing the interference. Typical approaches to SI mitigation therefore include precoding at the transmitter [4], analog-domain cancellation at the receiver [5], and improving spatial isolation between transmit and receive antennas through *antenna array design*. Indeed, the relative placement of the transmit (Tx) and receive (Rx) antennas fundamentally controls SI. In [6], the receive antenna is placed between two transmit antennas such that the two transmitted signals sum up destructively in the receive antenna. The geometry does not scale up to large antenna arrays, but in general, a favorable joint Tx-Rx array geometry can reduce—potentially even eliminate—the need for additional SI cancellation, reducing hardware costs and freeing up resources for communications tasks [7]. SI mitigation via array design holds great promise in future 6G and beyond massive MIMO systems, which offer an unprecedented number of degrees of freedom to shape the SI channel due to the hundreds or even thousands of antennas envisioned to be employed at a single BS [8].

Several questions nevertheless remain unanswered regarding the impact of the array geometry on SI. For instance: *which array geometries achieve low SI and why?* An obvious solution to reducing SI is to space the Tx and Rx arrays sufficiently far apart. However, this may be infeasible in practice due to only a limited aperture or area being available for placing the antenna elements. Placing all Tx and Rx antennas as far away as possible from each other may also be undesirable due to the resulting inefficient utilization of the available aperture/area, which a judicious *sparse array* could leverage to improve the angular resolution [9] of both the Tx and Rx arrays. The question, therefore, arises *whether there are array geometries that can simultaneously achieve high spatial resolution and low SI?* Angular resolution is increasingly important in future generation wireless systems operating at ever higher frequencies, where line-of-sight channel conditions are prevalent and scattering is sparse. Finally, for full-duplex massive MIMO systems employing large arrays, it becomes important to understand how SI scales with the number of antennas and aperture of the joint Tx-Rx array. Specifically, *does SI necessarily increase with a growing number of antennas?*

**Contributions:** This paper investigates how the array geometry impacts SI in full-duplex communications. We study

a commonly considered idealized SI channel model and two elementary array configurations that are indicative of the best and worst-case SI within the class of linear arrays. We show that the SI channel matrix has a simple Toeplitz structure in case of both arrays. This paves the way for analytically characterizing the SI of a multitude of geometries, such as the nested array [10], which we demonstrate can be adapted to the full-duplex setting to achieve both low SI and high angular resolution without ambiguities. We establish that the worst-case SI of the nested array need not increase with the number of antennas, but can actually decrease, provided the aperture also scales appropriately. This suggests that full-duplex massive MIMO systems with a large number of antennas may achieve negligible SI through array design alone.

**Notation:** Multiplication and addition of a set  $\mathbb{X}$  and scalar  $c \in \mathbb{R}$  are defined as  $c\mathbb{X} = \{cx, x \in \mathbb{X}\}$  and  $\mathbb{X} + c = \{x + c, x \in \mathbb{X}\}$ , respectively. The largest (smallest) element of  $\mathbb{X} \subset \mathbb{R}$  is denoted by  $\max \mathbb{X}$  ( $\min \mathbb{X}$ ). The set of the  $N$  first non-negative integers is denoted by  $\mathbb{U}_N \triangleq \{0, 1, \dots, N-1\}$ .

## 2. SIGNAL MODEL

Consider a full-duplex base station (BS) with  $N_t$  transmit (Tx) and  $N_r$  receive (Rx) antennas. The BS simultaneously serves  $D$  downlink (DL) and  $U$  uplink (UL) users using the same spectral resources. Assuming a narrowband model, the received signal at the BS (UL model) can be written as

$$\mathbf{y} = \mathbf{G}\mathbf{x} + \mathbf{H}\mathbf{s} + \mathbf{n}, \quad (1)$$

where  $\mathbf{x} \in \mathbb{C}^U$  is the symbol vector transmitted by the UL users,  $\mathbf{s} \in \mathbb{C}^{N_t}$  the DL signal transmitted by the BS, and  $\mathbf{n} \in \mathbb{C}^{N_r}$  denotes receiver noise. Furthermore,  $\mathbf{G} \in \mathbb{C}^{N_r \times U}$  is the UL channel matrix, and  $\mathbf{H} \in \mathbb{C}^{N_r \times N_t}$  is the *self-interference channel matrix*, of principle interest herein.

### 2.1. Self-interference model

We consider a simple spherical wave SI model, where the  $(n, m)$ th entry of  $\mathbf{H}$  can be written as [11]<sup>1</sup>

$$H_{n,m} = \rho \frac{\exp(j\pi\Delta_{n,m})}{\Delta_{n,m}}. \quad (2)$$

Here,  $\Delta_{n,m} \triangleq |d_r[n] - d_t[m]|$  denotes the distance between the  $n$ th Rx antenna  $d_r[n]$  and  $m$ th Tx antenna  $d_t[m]$  in units of  $\lambda/2$ , where  $\lambda$  is the carrier wavelength. Consequently,  $\mathbf{H} = \mathbf{H}(\mathbb{D}_r, \mathbb{D}_t)$  is a function of the Tx and Rx array geometries  $\mathbb{D}_t \triangleq \{d_t[m]\}_{m=1}^{N_t}$  and  $\mathbb{D}_r \triangleq \{d_r[n]\}_{n=1}^{N_r}$ , which, for simplicity, we assume to be one-dimensional and collinear. Moreover,  $\rho = \rho(\mathbb{D}_r, \mathbb{D}_t) > 0$  is a positive scaling factor, which may depend on the array geometry. Eq. (2) is representative of SI in antenna arrays with omnidirectional elements,

<sup>1</sup>Models similar to (2) have also been used for characterizing short-range MIMO communications channels [12] and mutual coupling [13].

such as ideal dipoles, in an anechoic environment. In other cases, deviation from (2) can be significant [14].

### 2.2. Objectives

The goal of the BS is to recover (decode) UL signal  $\mathbf{x}$ . This task is complicated by the simultaneous transmission of DL signal  $\mathbf{s}$ , which couples back to the BS receiver. Indeed, SI signal  $\mathbf{H}\mathbf{s}$  can be much stronger than received signal  $\mathbf{G}\mathbf{x}$ . The objective of this paper is to *gain an understanding of how matrix  $\mathbf{H}$  can be favorably shaped by antenna array design to mitigate SI*. More formally, an ideal  $\mathbf{H}$  would have a negligible worst-case SI with respect to the magnitude of the received signal of interest:  $\|\mathbf{H}\|_2\|\mathbf{s}\|_2 \ll \|\mathbf{G}\mathbf{x}\|_2$ . Alternatively, an approximately low rank  $\mathbf{H}$  may suffice such that most choices of  $\mathbf{s}$  within some signal class of interest yield a small SI:  $\|\mathbf{H}\mathbf{s}\|_2 \ll \|\mathbf{G}\mathbf{x}\|_2 \forall \mathbf{s} \in \mathcal{S} \subset \mathbb{C}^{N_t}$ . For example,  $\mathcal{S}$  could represent a Tx beamforming codebook designed for a millimeter-wave full-duplex communication system [11, 15].<sup>2</sup> Achieving either of these objectives by array design alone reduces the need for additional SI mitigation, which could potentially save both hardware and computational resources.

## 3. IMPACT OF ARRAY GEOMETRY ON SELF-INTERFERENCE

This section examines the structure of the SI matrix (2) in case of two elementary Tx-Rx array geometries denoted as the “partitioned” and “interleaved” arrays. This provides a preliminary understanding of how the joint Tx-Rx array geometry influences SI. For ease of exposition, we henceforth assume an equal number of Tx and Rx antennas  $N = N_r = N_t$ .

### 3.1. Structure of self-interference matrix

We define the partitioned and interleaved arrays as follows:

Partitioned array (with parameter  $\delta_1 \in \mathbb{N}$ ):

$$\begin{aligned} \mathbb{D}_r &= \mathbb{P}_r \triangleq \mathbb{U}_N \\ \mathbb{D}_t &= \mathbb{P}_t \triangleq \mathbb{P}_r + N + \delta_1, \end{aligned} \quad (3)$$

Interleaved array (with parameter  $\delta_2 \in \mathbb{N}_+$ ):

$$\begin{aligned} \mathbb{D}_r &= \mathbb{I}_r \triangleq 2\delta_2\mathbb{U}_N \\ \mathbb{D}_t &= \mathbb{I}_t \triangleq \mathbb{I}_r + \delta_2. \end{aligned} \quad (4)$$

In (3), the joint Tx-Rx array is divided (partitioned) into two uniform linear arrays (ULAs), which are separated by  $\delta_1$ . Similarly, in (4), the joint array geometry consists of alternating (interleaved) Tx and Rx antennas uniformly separated

<sup>2</sup>Similar conclusions hold for Rx beamforming (either in the digital or analog domain). Note that (1) implicitly assumes a fully digital Rx architecture.

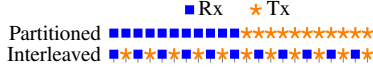


**Fig. 1.** Partitioned and interleaved array geometries in (3) and (4) with  $N = 11$  Tx/Rx antennas ( $\delta_1 = 0, \delta_2 = 1$ ).

by  $\delta_2$  (in units of  $\lambda/2$ ). The partitioned and interleaved array configurations are depicted in Fig. 1 for  $N = 11$  Tx/Rx antennas, and parameters  $\delta_1 = 0, \delta_2 = 1$ .

The partitioned array is widely considered in the full-duplex literature, in part due to its favorable SI compared to other linear arrays of equal aperture and with the same number of antennas [7]. Hence, the partitioned array seems to be representative of the best-case linear geometry in terms of SI. In contrast, the interleaved array has been observed to suffer from high SI [7], thus representing a worst-case linear array geometry in terms of SI. While the interleaved array is rarely employed in practice, it provides a useful model for investigating the spectral properties of  $\mathbf{H}$ , as we will see next. Indeed,  $\mathbf{H}$  in (2) becomes a real-valued Toeplitz matrix in case of both the partitioned and interleaved arrays. Specifically,  $\mathbf{H}$  can be approximately low-rank for the partitioned array, whereas this is the case for the interleaved array.

### 3.1.1. Partitioned array

In case of the partitioned array (3), the distances between Tx-Rx antenna pairs form the following  $N \times N$  Toeplitz matrix:

$$\Delta(\mathbb{P}_r, \mathbb{P}_t) = \delta_1 + \begin{bmatrix} N & N+1 & \dots & 2N-1 \\ N-1 & N & & 2N-2 \\ \vdots & & \ddots & \vdots \\ 1 & 2 & \dots & N \end{bmatrix}.$$

Hence,  $\mathbf{H}$  in (2) is also a (real-valued) Toeplitz matrix:

$$\mathbf{H}(\mathbb{P}_r, \mathbb{P}_t) = (-1)^{\delta_1} \rho_1 \begin{bmatrix} \frac{(-1)^N}{N+\delta_1} & \frac{(-1)^{N+1}}{N+1+\delta_1} & \dots & \frac{-1}{2N-1+\delta_1} \\ \frac{(-1)^{N-1}}{N-1+\delta_1} & \frac{(-1)^N}{N+\delta_1} & \dots & \frac{1}{2N-2+\delta_1} \\ \vdots & \vdots & \ddots & \vdots \\ \frac{-1}{1+\delta_1} & \frac{1}{2+\delta_1} & \dots & \frac{(-1)^N}{N+\delta_1} \end{bmatrix},$$

for some  $\rho_1 > 0$ . The sign of the entries in  $\mathbf{H}$  alternates due to  $\Delta$  consisting of consecutive integers  $n = 1, 2, \dots, 2N-1$  and the phase term in (2) being of the form  $e^{j\pi n} = (-1)^n$ .

### 3.1.2. Interleaved array

In case of the interleaved array, distance matrix  $\Delta \in \mathbb{N}_+^{N \times N}$  is again Toeplitz due to the regular structure of the array:

$$\Delta(\mathbb{I}_r, \mathbb{I}_t) = \delta_2 \begin{bmatrix} 1 & 3 & 5 & \dots & 2N-1 \\ 1 & 1 & 3 & & 2N-3 \\ 3 & 1 & 1 & & 2N-5 \\ \vdots & & & \ddots & \vdots \\ 2N-3 & 2N-5 & 2N-7 & \dots & 1 \end{bmatrix}.$$

Similarly,  $\mathbf{H}$  is also a real Toeplitz matrix (for any  $\rho_2 > 0$ ):

$$\mathbf{H}(\mathbb{I}_r, \mathbb{I}_t) = \frac{(-1)^{\delta_2} \rho_2}{\delta_2} \begin{bmatrix} 1 & \frac{1}{3} & \frac{1}{5} & \dots & \frac{1}{2N-1} \\ 1 & 1 & \frac{1}{3} & \dots & \frac{1}{2N-3} \\ \frac{1}{3} & 1 & 1 & \dots & \frac{1}{2N-5} \\ \vdots & & & \ddots & \vdots \\ \frac{1}{2N-3} & \frac{1}{2N-5} & \frac{1}{2N-7} & \dots & 1 \end{bmatrix}.$$

All entries in  $\mathbf{H}$  have the same sign since  $\Delta$  consists of only odd or even integers depending on the value of  $\delta_2 \in \mathbb{N}_+$ .

The structure of  $\mathbf{H}$  in case of the partitioned and interleaved arrays can be leveraged to gain insight into the fundamental dependence of SI on array geometry. Towards this goal, the next section inspects the scaling of the smallest and largest singular values of  $\mathbf{H}$  when  $N = 2$ . This case study conveys the basic intuition behind why the partitioned array has a more favorable SI than the interleaved array. Extensions to arbitrary values of  $N$  will be part of future work.

## 3.2. Self-interference in case of $N = 2$ Tx & Rx antennas

When the Tx and Rx arrays both have two antennas each ( $N = 2$ ), the SI matrices of the partitioned and interleaved arrays, respectively, become

$$\mathbf{H}(\mathbb{D}_t, \mathbb{D}_r) = \begin{cases} (-1)^{\delta_1} \rho_1 \begin{bmatrix} \frac{1}{2+\delta_1} & \frac{-1}{3+\delta_1} \\ \frac{-1}{1+\delta_1} & \frac{1}{2+\delta_1} \end{bmatrix}, & \text{if } \begin{cases} \mathbb{D}_t = \mathbb{P}_t \\ \mathbb{D}_r = \mathbb{P}_r \end{cases} \\ \frac{(-1)^{\delta_2} \rho_2}{\delta_2} \begin{bmatrix} 1 & \frac{1}{3} \\ 1 & 1 \end{bmatrix}, & \text{if } \begin{cases} \mathbb{D}_t = \mathbb{I}_t \\ \mathbb{D}_r = \mathbb{I}_r \end{cases} \end{cases}$$

For large values of  $\delta_1$ ,  $\mathbf{H}$  becomes approximately rank-1 in case of the partitioned array as  $\mathbf{H}(\mathbb{P}_t, \mathbb{P}_r) \approx (-1)^{\delta_1} \rho_1 [\mathbf{h}, -\mathbf{h}]$ , where  $\mathbf{h} = \frac{1}{\delta_1} [1, -1]^\top$ . In contrast, the SI matrix of the interleaved array has full rank; in particular, the smallest and largest singular values are proportional to each other regardless of the value of  $\delta_2$ .<sup>3</sup> This aligns with the intuition that when the separation between the Tx and Rx antennas grows large, all Rx antennas of the partitioned array observe the same *single* plane wave originating from the direction of the Tx antennas, whereas for the interleaved array, all Rx antennas except one observe *two* plane waves—one impinging from  $-\pi/2$  and the other from  $\pi/2$ —since Tx antennas are located on both sides of these Rx antennas. This is also known as *angular spread*—see [7] and references therein.

## 4. SPARSE ARRAYS IN FULL-DUPLEX MASSIVE MIMO COMMUNICATIONS

This section demonstrates how judicious sparse array designs can yield both *low SI* and *high angular resolution* in full-duplex systems employing a large number of antennas. We

<sup>3</sup>The singular values of  $\mathbf{H}(\mathbb{I}_t, \mathbb{I}_r)$  for  $N = 2$  can be verified to be  $\sqrt{(14 + 4\sqrt{10})/9} \frac{\rho_2}{\delta_2} \approx 1.7 \frac{\rho_2}{\delta_2}$  and  $\sqrt{(14 - 4\sqrt{10})/9} \frac{\rho_2}{\delta_2} \approx 0.4 \frac{\rho_2}{\delta_2}$ .

explore the scaling of  $\|\mathbf{H}\|_2$ , which controls the worst-case SI, as a function of the number of antennas and array aperture. Contrary to Section 3, the entries of  $\mathbf{H}$  are obtained from the S-parameters—simulated via the MATLAB antenna toolbox [16]—of the  $N_r \times N_t$ -port system corresponding to the joint Tx-Rx antenna array, assumed to consist of ideal strip dipole antennas (of length  $\lambda/2$  and width  $\lambda/100$ ) in an anechoic environment. Future work will investigate the scaling of SI using (2), which may also require modeling scalar  $\rho$ .

#### 4.1. Nested full-duplex array: Low self-interference and high resolution without ambiguities

Increasing the array aperture for a fixed number of (Tx and Rx) antennas has two key advantages. Firstly, it can decrease SI. Secondly, the increased aperture enables enhancing angular resolution. However, leveraging both reduced SI and increased aperture requires judiciously designing the joint Tx-Rx array geometry. Indeed, both the partitioned and interleaved arrays fall short in this aspect: in case of the partitioned array, both the Rx and Tx array apertures ( $\max \mathbb{D}_r - \min \mathbb{D}_r$  and  $\max \mathbb{D}_t - \min \mathbb{D}_t$ ) are fixed regardless of the effective aperture of the joint Tx-Rx array  $L \triangleq \max \mathbb{D}_t - \min \mathbb{D}_r$ ; in case of the interleaved array, the uniform sub-sampling of the Tx and Rx arrays gives rise to grating lobes, which in turn lead to angular ambiguities. The limited resolution of the partitioned array and the grating lobes of the interleaved array can be overcome by employing a sparse array geometry, such as the following variation of the widely-known *nested array* [10]:

Nested (full-duplex) array (with parameters  $M_1, M_2, \delta_3 \in \mathbb{N}_+$ )

$$\begin{aligned} \mathbb{D}_r &= \mathbb{S}_r \triangleq \mathbb{U}_{M_1} \cup (2\delta_3(\mathbb{U}_{M_2} + 1) + M_1 - 1) \\ \mathbb{D}_t &= \mathbb{S}_t \triangleq \max \mathbb{S}_r - \mathbb{S}_r + M_1 - 1 + \delta_3. \end{aligned} \quad (5)$$

Here,  $M_1, M_2$  are positive integers satisfying  $N = M_1 + M_2$  for a given  $N$ , and  $\delta_3$  controls the inter-sensor spacing of the sparse ULA. The nested array can be seen as a mixture of the partitioned and interleaved arrays, as illustrated in Fig. 2 (top) for  $N = 11$  and parameter values  $\delta_1 = 23, \delta_2 = 2, M_1 = 6, M_2 = 5, \delta_3 = 3$ . The nested array leverages the full aperture  $L$  of the joint Tx-Rx array to achieve a narrow (Tx or Rx) main beam without introducing angular ambiguities via high side lobes (Fig. 2, center). It also strikes a balance between the SI of the partitioned and interleaved arrays, as evidenced by the singular values of  $\mathbf{H}$  shown in the bottom plot of Fig. 2. The transparent lines correspond to the spherical wave model in (2) with  $\rho = 0.2$ . The agreement with the electromagnetic solver (solid markers) is apparent, which further validates the physical relevance of (2).

Finally, we note that when  $L \propto N^2$ , the nested full-duplex array can also be verified to yield on the order of  $N^2$  contiguous *virtual* Tx-Rx antennas in its so-called *sum co-array*. The

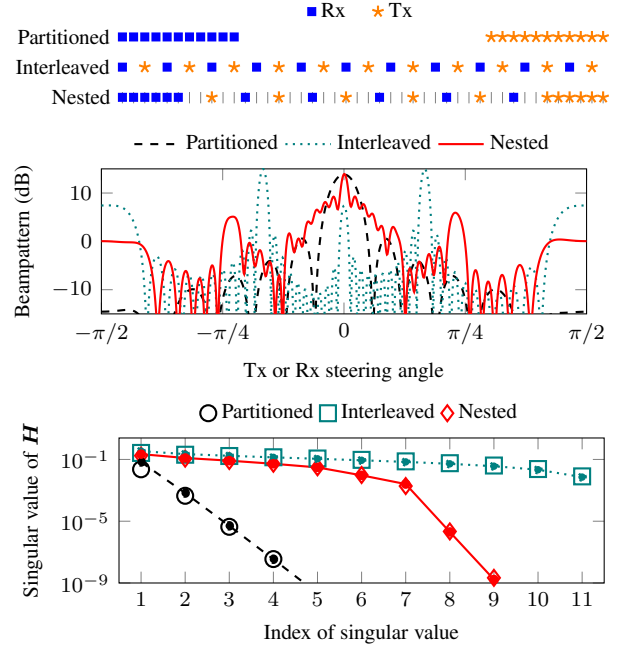


**Fig. 2.** The nested full-duplex array leverages the full aperture of the joint Tx-Rx array (top) to achieve a narrow Tx/Rx main lobe width (mid) and SI between that of the partitioned and interleaved arrays (bottom). The SI of the simulated dipole array is well approximated by the spherical wave model (2) (bottom: solid marks vs. transparent lines) ( $N = 11, \delta_1 = 23, \delta_2 = 2, M_1 = 6, M_2 = 5, \delta_3 = 3$ ).

sum co-array [17] is a virtual array arising in active sensing systems with co-located transmitters and receivers. The large contiguous co-array guarantees the identifiability of  $\mathcal{O}(N^2)$  scatterers/targets, which is desirable when the BS also performs sensing, as is the case in dual-function ISAC systems.

#### 4.2. Scaling of self-interference with $N$

Fig. 3 shows the largest singular value of  $\mathbf{H}$  as a function of the number of Tx/Rx antennas  $N$  for two different aperture scaling laws,  $L \propto N$  and  $L \propto N^2$ . The regime of large  $N$  and  $L$  is of interest in future wireless systems requiring high spatial resolution.<sup>4</sup> When  $L \propto N$ ,  $\|\mathbf{H}\|_2$  only weakly depends on  $N$ . However, as  $L \propto N^2$ ,  $\|\mathbf{H}\|_2$  decreases with  $N$  since the separation between *any* Tx-Rx antenna pair also increases in case of the three considered array geometries. This suggests that massive MIMO systems can actually mitigate SI more effectively when the number of antennas increases by virtue of judicious array design alone.

<sup>4</sup>When  $L \propto N^2$ , the main lobe width of the Tx/Rx array beam pattern is proportional to  $1/N^2$  in case of the nested and interleaved arrays, whereas it is only proportional to  $1/N$  in case of the partitioned array.

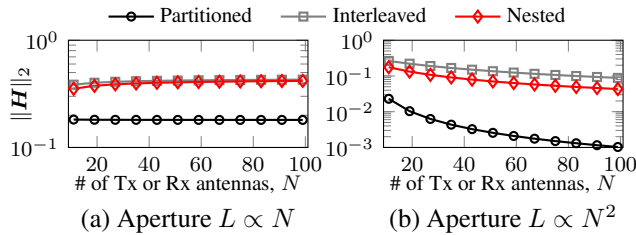


**Fig. 3.** The largest singular value of  $\mathbf{H}$  can decrease with the number of Tx/Rx antennas  $N$  if the aperture  $L$  grows suitably with  $N$  and the array geometry is such that the spacing between each Tx-Rx antenna pair also increases with  $N$ .

## 5. CONCLUSIONS

This paper investigated the impact of the array geometry on self-interference (SI) in wireless full-duplex systems. We showed that a simple spherical-wave model can provide insight into the degree of SI caused by different array geometries. Specifically, the SI matrix assumes a simple Toeplitz structure in case of certain elementary array configurations consisting of ULAs (including uniformly subsampled ones). Hence, it becomes possible to analytically characterize the spectral properties of the SI matrix, which can provide a preliminary understanding of the SI experienced by different array geometries as a function of aperture and the number of antennas. We demonstrated that judicious sparse array designs, such as the nested array, are able to leverage an increased joint Tx-Rx aperture for achieving both low self-interference and high angular resolution (upon both Tx and Rx). Simulations showed that SI can decrease with an increasing number of Tx/Rx antennas for such sparse arrays. Future work will examine SI in case of both one and two-dimensional array geometries at depth.

## 6. REFERENCES

- [1] A. Sabharwal, P. Schniter, D. Guo, D. W. Bliss, S. Rangarajan, and R. Wichman, "In-band full-duplex wireless: Challenges and opportunities," *IEEE Journal on Selected Areas in Communications*, vol. 32, no. 9, pp. 1637–1652, 2014.
- [2] G. C. Alexandropoulos, M. A. Islam, and B. Smida, "Full-duplex massive multiple-input, multiple-output architectures: Recent advances, applications, and future directions," *IEEE Vehicular Technology Magazine*, vol. 17, no. 4, pp. 83–91, 2022.
- [3] C. B. Barneto, S. D. Liyanaarachchi, M. Heino, T. Riihonen, and M. Valkama, "Full duplex radio/radar technology: The enabler for advanced joint communication and sensing," *IEEE Wireless Communications*, vol. 28, no. 1, pp. 82–88, 2021.
- [4] T. Riihonen, S. Werner, and R. Wichman, "Mitigation of loopback self-interference in full-duplex MIMO relays," *IEEE Transactions on Signal Processing*, vol. 59, no. 12, pp. 5983–5993, 2011.
- [5] K. E. Kolodziej, B. T. Perry, and J. S. Herd, "In-band full-duplex technology: Techniques and systems survey," *IEEE Transactions on Microwave Theory and Techniques*, vol. 67, no. 7, pp. 3025–3041, 2019.
- [6] J. I. Choi, M. Jain, K. Srinivasan, P. Levis, and S. Katti, "Achieving single channel, full duplex wireless communication," in *Proceedings of the Sixteenth Annual International Conference on Mobile Computing and Networking*, 2010.
- [7] E. Everett, C. Shepard, L. Zhong, and A. Sabharwal, "Softnull: Many-antenna full-duplex wireless via digital beamforming," *IEEE Transactions on Wireless Communications*, vol. 15, no. 12, pp. 8077–8092, 2016.
- [8] E. G. Larsson, O. Edfors, F. Tufvesson, and T. L. Marzetta, "Massive MIMO for next generation wireless systems," *IEEE Communications Magazine*, vol. 52, no. 2, pp. 186–195, 2014.
- [9] P. Sarangi, M. C. Hücumenoğlu, R. Rajamäki, and P. Pal, "Super-resolution with sparse arrays: A non-asymptotic analysis of spatio-temporal trade-offs," *IEEE Transactions on Signal Processing*, pp. 1–14, 2023.
- [10] P. Pal and P. P. Vaidyanathan, "Nested arrays: A novel approach to array processing with enhanced degrees of freedom," *IEEE Transactions on Signal Processing*, vol. 58, no. 8, pp. 4167–4181, Aug 2010.
- [11] I. P. Roberts, S. Vishwanath, and J. G. Andrews, "LoneSTAR: Analog beamforming codebooks for full-duplex millimeter wave systems," *IEEE Transactions on Wireless Communications*, vol. 22, no. 9, pp. 5754–5769, 2023.
- [12] J.-S. Jiang and M. Ingram, "Spherical-wave model for short-range MIMO," *IEEE Transactions on Communications*, vol. 53, no. 9, pp. 1534–1541, 2005.
- [13] C.-L. Liu and P. P. Vaidyanathan, "Super nested arrays: Linear sparse arrays with reduced mutual coupling – Part I: Fundamentals," *IEEE Transactions on Signal Processing*, vol. 64, no. 15, pp. 3997–4012, Aug 2016.
- [14] I. P. Roberts, A. Chopra, T. Novlan, S. Vishwanath, and J. G. Andrews, "Spatial and statistical modeling of multi-panel millimeter wave self-interference," *IEEE Journal on Selected Areas in Communications*, vol. 41, no. 9, pp. 2780–2795, 2023.
- [15] I. P. Roberts, J. G. Andrews, H. B. Jain, and S. Vishwanath, "Millimeter-wave full duplex radios: New challenges and techniques," *IEEE Wireless Communications*, vol. 28, no. 1, pp. 36–43, 2021.
- [16] I. The MathWorks, *Antenna Toolbox, MATLAB version 9.13.0.2105380 (R2022b)*, Natick, MA, USA, 2022.
- [17] R. T. Hoctor and S. A. Kassam, "The unifying role of the coarray in aperture synthesis for coherent and incoherent imaging," *Proceedings of the IEEE*, vol. 78, no. 4, pp. 735–752, Apr 1990.